JOURNAL OF THEORETICAL AND APPLIED MECHANICS
57, 1, pp. 221-233, Warsaw 2019
DOI: 10.15632/jtam-pl.57.1.221

NATURAL AND MIXED CONVECTION OF A NANOFLUID IN POROUS CAVITIES: CRITICAL ANALYSIS USING BUONGIORNO'S MODEL

Iman Zahmatkesh, Mohammad Reza Habibi
Department of Mechanical Engineering, Mashhad Branch, Islamic Azad University, Mashhad, Iran
e-mail: zahmatkesh5310@mshdiau.ac.ir

In this paper, Buongiorno's mathematical model is adopted to simulate both natural convection and mixed convection of a nanofluid in square porous cavities. The model takes into account the Brownian diffusion and thermophoresis effects. Both constant and variable temperatures are prescribed at the side walls while the remaining walls are maintained adiabatic. Moreover, all boundaries are assumed to be impermeable to the base fluid and the nanoparticles. The governing equations are transformed to a form of dimensionless equations and then solved numerically using the finite-volume method. Thereafter, effects of the Brownian diffusion parameter, the thermophoresis number, and the buoyancy ratio on the flow strength and the average Nusselt number as well as distributions of isocontours of the stream function, temperature, and nanoparticles fraction are presented and discussed.

Keywords: natural convection, mixed convection, nanofluid, porous media, Buongiorno's model

1. Introduction

Heat transfer is a significant and widely explored engineering problem that, due to the lack of energy resources, has become truly important. One efficient way to improve heat transfer and to reduce energy consumption goes back to the use of porous media. This occurs since a porous medium provides a large surface area for heat exchange. On the other hand, the flow field in a porous medium is completely three-dimensional and irregular, which intensifies fluid mixing.

Further attempt to achieve higher heat transfer rates has led to adding nanoparticles to working liquids and producing nanofluids. The added nanoparticles are usually made up of metals or metal oxides with high thermal conductivity. So, the resulting fluid has a better thermal efficiency than the base liquid. Going into the literature, one may find that heat transfer analysis of nanofluid flows has been a hot topic among scientists over the past decade. Examples include the studies of Ali *et al.* (2014), Ghasemi *et al.* (2016), and Rostamzadeh *et al.* (2016).

Different mathematical models have been adopted to describe heat transfer in nanofluids. The simplest method with the least computational burden is the homogenous model. In this model, the concentration of nanoparticles is taken constant over the entire flow field. It is also assumed that the base liquid and the nanoparticles are in local equilibrium and move with the same velocity and temperature. In spite of previous achievements of this model, some studies have proved that more complex models provide better agreement with experimental data (e.g., Behroyan *et al.* (2016); Torshizi and Zahmatkesh, 2016).

Buongiorno (2006) introduced seven transport mechanisms which cause relative velocity between the nanoparticles and the base liquid, namely, inertia, Brownian diffusion, thermophoresis, diffusiophoresis, Magnus effect, fluid drainage, and gravitational settling. After comparing the diffusion time scales of these mechanisms he drew a conclusion that, in the absence of flow turbulence, the Brownian diffusion and thermophoresis are the most important effects. Based on this finding, he then developed a non-homogeneous but an equilibrium model for nanofluid flow

and heat transfer that incorporates the effects of the Brownian diffusion and thermophoresis. The Brownian diffusion occurs due to random variations in the bombardment of the base fluid molecules against the particles. The thermophoresis phenomenon appears as a net force acting in the opposite direction to the gradient of temperature and is a direct result of the differential bombardment of the base fluid molecules in the vicinity of the particles (Zahmatkesh, 2008b).

There are many recent papers that deal with Buongiorno's mathematical model (e.g., Sheikholeslami *et al.*, 2016; Kefayati, 2017a; Mustafa, 2017) but to the best of our knowledge, there are no previous works in literature which compare the role of parameters appearing in this model for both natural convection and mixed convection in porous media. Some simulation studies for natural convection of nanofluids in porous cavities based on Buongiorno's model are discussed below.

Sheremet *et al.* (2014) simulated natural convection of nanofluids in shallow and slender porous cavities. Their results demonstrated that an inverse relation existed between the average Nusselt number and the buoyancy ratio. Conjugate natural convection of nanofluid in a square porous cavity was discussed by Sheremet and Pop (2014a). They found that the Nusslet number was an increasing function of the buoyancy ratio and a decreasing function of the thermophoresis number and the Lewis number. A simulation study of natural convection of a nanofluid in a right-angle triangular porous cavity was reported by Sheremet and Pop (2015a). That investigation showed that the average Nusselt number increased with the enhancement of the Lewis number but any rise in the Brownian diffusion parameter, the buoyancy ratio or the thermophoresis number made it lower. Sheremet *et al.* (2015) discussed natural convection heat transfer of a nanofluid in a three-dimensional porous cavity. Their results led to the conclusion that the average Nusselt number increased with the Brownian diffusion parameter and decreased with the buoyancy ratio and the thermophoresis number. Sheremet and Pop (2015b) analyzed natural convection of a nanofluid in a porous annulus. They indicated that an increase in the thermophoresis number and the buoyancy ratio led to deterioration in the average Nusselt number while the Brownian diffusion parameter contributed neutrally. Ghalambaz *et al.* (2016) investigated the influence of viscous dissipation and radiation on natural convection of a nanofluid in a porous cavity and concluded that an increase in the Lewis number improved the heat transfer but augmentation of the buoyancy ratio and the thermophoresis number decreased it. More recently, natural convection and entropy generation of a non-Newtonian nanofluid in a porous cavity was pointed out by Kefayati (2017b). The results demonstrated that rise of the Lewis number, the thermophoresis number, and the Brownian diffusion parameter declined the average Nusselt number, but the augmentation of the buoyancy ratio enhanced it.

The role of parameters appearing in Buongiorno's mathematical model may depend on thermal boundary conditions of the cavity. In this context, Sheremet and Pop (2014b) discussed how imposition of a sinusoidal temperature distribution on the side walls may affect natural convection of the nanofluid in a square porous cavity. They found that the average Nusselt number was an increasing function of the buoyancy ratio and the thermophoresis number but a decreasing function of the Lewis number and the Brownian diffusion parameter. More recently, they extended their work to a wavy porous cavity (Sheremet *et al.*, 2017). They found that the dependence of the average Nusselt number to the pertinent parameters was similar to the square cavity, which was in contrast to the aforesaid findings in uniformly heated/cooled cavities.

The current research deals with heat transfer of a nanofluid in square porous cavities. The main purpose of this article is to analyze the effects of the buoyancy ratio, the Brownian diffusion parameter and the thermophoresis number on the flow strength and the average Nusselt number as well as developments of streamlines, isotherms and isoconcentrations. To provide a critical analysis, computations are undertaken for various cases in natural convection and mixed convection environments with both uniform and non-uniform wall temperatures.

2. Problem definition and mathematical formulation

Both natural and mixed convection heat transfer in a square cavity filled with a nanofluid-saturated porous medium are analyzed in this study. A schematic diagram of the flow problems is shown in Fig. 1, where x and y are the Cartesian coordinates and L is the size of the cavity. Here, all walls are assumed to be impermeable to mass transfer. The horizontal walls are assumed adiabatic while two different conditions are imposed on the side walls. In the first case, the sidewalls are considered to be heated/cooled uniformly while in the second case, the sidewalls are influenced by the existence of a sinusoidal temperature variation.

In this paper, Buongiorno's mathematical model is used. Thanks to this approach, the nanofluid is considered as a two-component dilute mixture. The porous medium is assumed isotropic and homogenous while the established flow is concerned to be steady, incompressible, Newtonian and laminar. The Darcy model is employed for the momentum equation. Moreover, a local thermal equilibrium is assumed between the nanoparticles, the base fluid and the porous medium. The Boussinesq approximation is adopted to determine the variations of density in the body force term within the momentum equation. Meanwhile, viscous dissipation, the work done by the pressure change and radiation heat transfer are neglected. Additionally, the thermophoresis and Brownian transport coefficients are assumed temperature-independent. On these assumptions, the conservation equations for mass, momentum, energy and flow concentration are (Nield and Bejan, 2013)

$$\begin{aligned}
&\nabla \cdot (\mathbf{V}) = 0\\
&\mathbf{0} = -\nabla P - \frac{\mu}{K}\mathbf{V} + [C\rho_p + (1-C)\rho_f(1-\beta(T-T_c))]\mathbf{g}\\
&\mathbf{V}\cdot\nabla T = \alpha_m \nabla^2 T + \delta\Big(D_B \nabla C\cdot\nabla T + \frac{D_T}{T_c}\nabla T\cdot\nabla T\Big)\\
&\frac{\rho_p}{\varepsilon}\mathbf{V}\cdot\nabla C = -\nabla\cdot\mathbf{j}_p
\end{aligned} \tag{2.1}$$

Here, $\mathbf{V}$ is the Darcy velocity vector, P is pressure, T is temperature, C is the nanoparticles fraction, $\mathbf{g}$ is gravitational acceleration ($\mathbf{g} = -g\mathbf{j}$), ρ is density, μ is dynamic viscosity, β is the volumetric expansion coefficient, α is thermal diffusivity, ε is medium porosity, and K is permeability of the porous medium. Meanwhile, D_B is the Brownian diffusion coefficient, D_T is the thermophoretic diffusion coefficient, and δ is a parameter defined by $\delta = \varepsilon(\rho c_p)_p/(\rho c_p)_f$ with c_p being the specific heat. Moreover, the subscripts p, f, and m correspond to the nanparticles, the base fluid and effective values, respectively.

In Eq. $(2.1)_4$, $\mathbf{j}_p$ is the nanoparticles mass flux. Based on Buongiorno's model, the nanoparticles mass flux is made up of two parts, namely, Brownian diffusion $\mathbf{j}_{p,B}$, and thermophoresis $\mathbf{j}_{p,T}$. Thus

$$\mathbf{j}_p = \mathbf{j}_{p,B} + \mathbf{j}_{p,T} = -\rho_p D_B \nabla C - \rho_p D_T \frac{\nabla T}{T} \tag{2.2}$$

After using the Boussinesq approximation and taking the nanofluid as a dilute mixture, one arrives at the following form of the momentum equation (Nield and Kuznetsov, 2009)

$$\mathbf{0} = -\nabla P - \frac{\mu}{K}\mathbf{V} + [C(\rho_p - \rho_{f_0}) + \rho_{f_0}(1-\beta(T-T_c)(1-C_0))]\mathbf{g} \tag{2.3}$$

with subscript 0 standing for reference values.

To simplify this vector equation, cross-differentiation is adopted, which eliminates the pressure term. So, the governing equations become

$$\frac{\partial u}{\partial x} + \frac{\partial v}{\partial y} = 0 \tag{2.4}$$

and

$$
\begin{aligned}
&0 = -\frac{\mu}{K}\Big(\frac{\partial u}{\partial y} - \frac{\partial v}{\partial x}\Big) + g(\rho_p - \rho_{f_0})\frac{\partial C}{\partial x} - (1-C_0)\rho_{f_0}\beta g\frac{\partial T}{\partial x}\\
&u\frac{\partial T}{\partial x} + v\frac{\partial T}{\partial y} = \alpha_m\Big(\frac{\partial^2 T}{\partial x^2} + \frac{\partial^2 T}{\partial y^2}\Big)\\
&\qquad + \delta\Big\{D_B\Big(\frac{\partial C}{\partial x}\frac{\partial T}{\partial x} + \frac{\partial C}{\partial y}\frac{\partial T}{\partial y}\Big) + \frac{D_T}{T_c}\Big[\Big(\frac{\partial T}{\partial x}\Big)^2 + \Big(\frac{\partial T}{\partial y}\Big)^2\Big]\Big\}\\
&\frac{1}{\varepsilon}\Big(u\frac{\partial C}{\partial x} + v\frac{\partial C}{\partial y}\Big) = D_B\Big(\frac{\partial^2 C}{\partial x^2} + \frac{\partial^2 C}{\partial y^2}\Big) + \frac{D_T}{T_c}\Big(\frac{\partial^2 T}{\partial x^2} + \frac{\partial^2 T}{\partial y^2}\Big)
\end{aligned}
\tag{2.5}
$$

where u and v denote the velocity components in the x and y directions, respectively.

After introducing the stream function by $u = \partial\psi/\partial y$ and $v = -\partial\psi/\partial x$, the continuity equation will be satisfied. Moreover, Eqs. (2.5) lead to

$$
\begin{aligned}
&\frac{\partial^2\psi}{\partial x^2} + \frac{\partial^2\psi}{\partial y^2} = -\frac{(1-C_0)\rho_{f_0}gK\beta}{\mu}\frac{\partial T}{\partial x} + \frac{\rho_p - \rho_{f_0}}{\mu}gK\frac{\partial C}{\partial x}\\
&\frac{\partial\psi}{\partial y}\frac{\partial T}{\partial x} - \frac{\partial\psi}{\partial x}\frac{\partial T}{\partial y} = \alpha_m\Big(\frac{\partial^2 T}{\partial x^2} + \frac{\partial^2 T}{\partial y^2}\Big)\\
&\qquad + \delta\Big\{D_B\Big(\frac{\partial C}{\partial x}\frac{\partial T}{\partial x} + \frac{\partial C}{\partial y}\frac{\partial T}{\partial y}\Big) + \frac{D_T}{T_c}\Big[\Big(\frac{\partial T}{\partial x}\Big)^2 + \Big(\frac{\partial T}{\partial y}\Big)^2\Big]\Big\}\\
&\frac{1}{\varepsilon}\Big(\frac{\partial\psi}{\partial y}\frac{\partial C}{\partial x} - \frac{\partial\psi}{\partial x}\frac{\partial C}{\partial y}\Big) = D_B\Big(\frac{\partial^2 C}{\partial x^2} + \frac{\partial^2 C}{\partial y^2}\Big) + \frac{D_T}{T_c}\Big(\frac{\partial^2 T}{\partial x^2} + \frac{\partial^2 T}{\partial y^2}\Big)
\end{aligned}
\tag{2.6}
$$

We now define the following parameters to make the above equations dimensionless

$$
\begin{aligned}
&X = \frac{x}{L} \qquad Y = \frac{y}{L} \qquad \Psi = \frac{\psi}{\alpha_m} \qquad \theta = \frac{T - T_c}{T_h - T_c}\\
&\Phi = \frac{C}{C_0} \qquad \mathrm{Ra} = \frac{(1-C_0)gK\rho_{f_0}\beta(T_h - T_c)L}{\alpha_m\mu}\\
&\mathrm{Pe} = \frac{V_0 L}{\alpha_m} \qquad \mathrm{Le} = \frac{\alpha_m}{\varepsilon D_B} \qquad Nb = \frac{\delta D_B C_0}{\alpha_m}\\
&Nr = \frac{(\rho_p - \rho_{f_0})C_0}{\rho_{f_0}\beta(T_h - T_c)(1-C_0)} \qquad Nt = \frac{\delta D_T(T_h - T_c)}{\alpha_m T_c}
\end{aligned}
\tag{2.7}
$$

Here, Ra is the Rayleigh number, Pe is the Peclet number (with V_0 being the inlet velocity), Le is the Lewis number, Nb is the Brownian diffusion parameter, Nr is the buoyancy ratio, and Nt is the thermophoresis number.

Substituting the dimensionless parameters into the governing equations yields

$$
\begin{aligned}
&\frac{\partial^2\Psi}{\partial X^2} + \frac{\partial^2\Psi}{\partial Y^2} = -\mathrm{Ra}\Big(\frac{\partial\theta}{\partial X} - Nr\frac{\partial\Phi}{\partial X}\Big)\\
&\frac{\partial\Psi}{\partial Y}\frac{\partial\theta}{\partial X} - \frac{\partial\Psi}{\partial X}\frac{\partial\theta}{\partial Y} = \frac{\partial^2\theta}{\partial X^2} + \frac{\partial^2\theta}{\partial Y^2} + Nb\Big(\frac{\partial\Phi}{\partial X}\frac{\partial\theta}{\partial X} + \frac{\partial\Phi}{\partial Y}\frac{\partial\theta}{\partial Y}\Big) + Nt\Big[\Big(\frac{\partial\theta}{\partial X}\Big)^2 + \Big(\frac{\partial\theta}{\partial Y}\Big)^2\Big]\\
&\mathrm{Le}\Big(\frac{\partial\Psi}{\partial Y}\frac{\partial\Phi}{\partial X} - \frac{\partial\Psi}{\partial X}\frac{\partial\Phi}{\partial Y}\Big) = \frac{\partial^2\Phi}{\partial X^2} + \frac{\partial^2\Phi}{\partial Y^2} + \frac{Nt}{Nb}\Big(\frac{\partial^2\theta}{\partial X^2} + \frac{\partial^2\theta}{\partial Y^2}\Big)
\end{aligned}
\tag{2.8}
$$

Notice that the governing equations reduce to those of a regular fluid if one chooses $Nb = Nr = Nt = 0$.

The boundary conditions for the flow problems are:

Case I: *Natural convection with a constant temperature at the side walls*

$$\begin{array}{lllll}
\text{Left wall:} & \Psi = 0 & \theta = 1 & j_p = 0\Big(or, Nb\dfrac{\partial \Phi}{\partial X} + Nt\dfrac{\partial \theta}{\partial X} = 0\Big) \\
\text{Right wall:} & \Psi = 0 & \theta = 0 & j_p = 0\Big(or, Nb\dfrac{\partial \Phi}{\partial X} + Nt\dfrac{\partial \theta}{\partial X} = 0\Big) \\
\text{Horizontal walls:} & \Psi = 0 & \dfrac{\partial \theta}{\partial Y} = 0 & \dfrac{\partial \Phi}{\partial Y} = 0
\end{array} \tag{2.9}$$

Case II: *Natural convection with a sinusoidal temperature distribution at the side walls*

$$\begin{array}{lllll}
\text{Left wall:} & \Psi = 0 & \theta = \sin(2\pi Y) & j_p = 0\Big(or, Nb\dfrac{\partial \Phi}{\partial X} + Nt\dfrac{\partial \theta}{\partial X} = 0\Big) \\
\text{Right wall:} & \Psi = 0 & \theta = \sin(2\pi Y) & j_p = 0\Big(or, Nb\dfrac{\partial \Phi}{\partial X} + Nt\dfrac{\partial \theta}{\partial X} = 0\Big) \\
\text{Horizontal walls:} & \Psi = 0 & \dfrac{\partial \theta}{\partial Y} = 0 & \dfrac{\partial \Phi}{\partial Y} = 0
\end{array} \tag{2.10}$$

Case III: *Mixed convection with a constant temperature at the side walls*

$$\begin{array}{lllll}
\text{Left wall:} & \Psi = 0.1\text{Pe} & \theta = 1 & j_p = 0\Big(or, Nb\dfrac{\partial \Phi}{\partial X} + Nt\dfrac{\partial \theta}{\partial X} = 0\Big) \\
\text{Right wall:} & \Psi = 0 & \theta = 0 & j_p = 0\Big(or, Nb\dfrac{\partial \Phi}{\partial X} + Nt\dfrac{\partial \theta}{\partial X} = 0\Big) \\
\text{Inlet:} & \Psi = Y\text{Pe} & \theta = 0 & \Phi = 1 \\
\text{Bottom wall:} & \Psi = 0 & \dfrac{\partial \theta}{\partial Y} = 0 & \dfrac{\partial \Phi}{\partial Y} = 0 \\
\text{Upper wall:} & \Psi = 0.1\text{Pe} & \dfrac{\partial \theta}{\partial Y} = 0 & \dfrac{\partial \Phi}{\partial Y} = 0 \\
\text{Outlet:} & \dfrac{\partial \Psi}{\partial X} = 0 & \dfrac{\partial \theta}{\partial X} = 0 & \dfrac{\partial \Phi}{\partial X} = 0
\end{array} \tag{2.11}$$

Case IV: *Mixed convection with a sinusoidal temperature distribution at the side walls*

$$\begin{array}{lllll}
\text{Left wall:} & \Psi = 0.1\text{Pe} & \theta = \sin(2\pi Y) & j_p = 0\Big(or, Nb\dfrac{\partial \Phi}{\partial X} + Nt\dfrac{\partial \theta}{\partial X} = 0\Big) \\
\text{Right wall:} & \Psi = 0 & \theta = \sin(2\pi Y) & j_p = 0\Big(or, Nb\dfrac{\partial \Phi}{\partial X} + Nt\dfrac{\partial \theta}{\partial X} = 0\Big) \\
\text{Inlet:} & \Psi = Y\text{Pe} & \theta = 0 & \Phi = 1 \\
\text{Bottom wall:} & \Psi = 0 & \dfrac{\partial \theta}{\partial Y} = 0 & \dfrac{\partial \Phi}{\partial Y} = 0 \\
\text{Upper wall:} & \Psi = 0.1\text{Pe} & \dfrac{\partial \theta}{\partial Y} = 0 & \dfrac{\partial \Phi}{\partial Y} = 0 \\
\text{Outlet:} & \dfrac{\partial \Psi}{\partial X} = 0 & \dfrac{\partial \theta}{\partial X} = 0 & \dfrac{\partial \Phi}{\partial X} = 0
\end{array} \tag{2.12}$$

The physical quantities related to the problems are the local and average Nusselt numbers $(\text{Nu}, \overline{\text{Nu}})$ and the local and average Sherwood numbers $(\text{Sh}, \overline{\text{Sh}})$ (Sheremet and Pop, 2014b)

$$\mathrm{Nu} = -\left.\frac{\partial\theta}{\partial X}\right|_{X=0} \qquad \overline{\mathrm{Nu}} = \frac{1}{0.9}\int_{0.1}^{1} \mathrm{Nu}\, dY$$
$$\mathrm{Sh} = -\left.\frac{\partial\Phi}{\partial X}\right|_{X=0} \qquad \overline{\mathrm{Sh}} = \frac{1}{0.9}\int_{0.1}^{1} \mathrm{Sh}\, dY \tag{2.13}$$

In the flow problems, we limit our attention to the Nusselt number since, at the side walls, we have $\mathrm{Sh} = -(Nt/Nb)\mathrm{Nu}$.

3. Solution method

The governing equations constitute a system of nonlinear partial differential equations. In order to discretize them, the finite-volume approach is adopted. By integrating the governing equations over each control volume, a system of algebraic equations is produced, which is solved by the Tri--Diagonal Matrix Algorithm (TDMA). Appropriate relaxation is chosen on the basis of numerical experiments. The iteration is terminated when changes between two consecutive iterations get smaller than 10^{-5}. The solution method has been implemented in FORTRAN software.

For the purpose of acquiring an acceptable grid for each current case, four different grid independence tests have been carried out. The results indicated that the suitable grid systems are 200×200 (Case I), 400×400 (Case II and Case III), and 300×300 (Case IV).

The employed Fortran code is essentially a modified version of a code built and validated in the previous works (Zahmatkesh, 2008a, 2015; Zahmatkesh and Naghedifar, 2017). In order to evaluate the accuracy of this code for simulation of nanofluid-saturated porous cavities with Buongiorno's model, the corresponding results have been compared with those of Sheremet *et al.* (2014) in Table 1. Here, the average Nusselt numbers in a square porous cavity with isothermal vertical walls and adiabatic horizontal walls saturated with the nanofluid are presented. The compared results belong to Ra = 100, Le = 1, 10, 100, $Nr = 0.1$, 0.4, and $Nb = Nt = 0.4$. Notice that there is a trustworthy similarity with that study. This assured us that our results are reliable. So, we have applied the code to analyze the flow problems depicted in Fig. 1.

Table 1. Comparison of the present results with those of previous works at Ra = 100

Le	Nr	$\overline{\mathrm{Nu}}$	
		Sheremet *et al.* (2014)	Current study
1	0.1	3.8387	3.8108
	0.4	2.7791	2.7617
10	0.1	4.6270	4.5575
	0.4	4.0088	3.9637
100	0.1	4.6252	4.4401
	0.4	4.3049	4.1542

4. Simulation results

In this Section, simulation results for both natural convection and mixed convection heat transfer of the nanofluid are presented. The results are discussed for the following values of the pertinent parameters: the Rayleigh number (Ra = 30, 100, 300), the Peclet number (Pe = 25), the Lewis number (Le = 25), the buoyancy ratio ($Nr = 0.05$, 0.1, 0.5), the Brownian diffusion parameter ($Nb = 0.05$, 0.1, 0.5) and the thermophoresis number ($Nt = 0.05$, 0.1, 0.5).

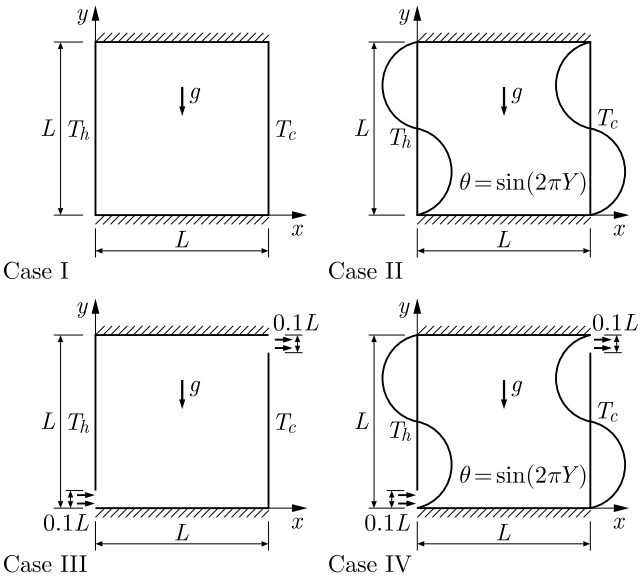

Fig. 1. Physical models of the flow problem: (a) Case I: Natural convection with a constant temperature at the side walls; (b) Case II: Natural convection with a sinusoidal temperature distribution at the side walls; (c) Case III: Mixed convection with a constant temperature at the side walls; (d) Case IV: Mixed convection with a sinusoidal temperature distribution at the side walls

Tables 2, 3, and 4 illustrate the numerical values of $|\Psi_{max}|$ and $\overline{\mathrm{Nu}}$ for the four configurations at Ra = 30, 100, 300, respectively. Here, $|\Psi_{max}|$ provides a measure of the convection vigor. In a general way, the imposition of the sinusoidal temperature distribution on the sidewalls leads to heat transfer enhancement both in the natural and mixed convection environments within the current range of the Rayleigh number. This imposition also intensifies the flow strength in the mixed convection case. In the natural convection problem, however, depending on the value of Ra, the sinusoidal wall temperature may enhance or deteriorate the flow strength.

Table 2. Numerical values of $|\Psi_{max}|$ and $\overline{\mathrm{Nu}}$ for the flow at Ra = 30

Ra = 30		Nb		Nr		Nt		$Nb = Nr = Nt$
		0.05	0.5	0.05	0.5	0.05	0.5	0.1
Case I	$\lvert\Psi_{max}\rvert$	1.909	1.918	1.916	1.894	1.917	1.889	1.914
	$\overline{\mathrm{Nu}}$	1.421	1.424	1.423	1.417	1.455	1.186	1.422
Case II	$\lvert\Psi_{max}\rvert$	0.750	0.750	0.750	0.750	0.736	0.878	0.750
	$\overline{\mathrm{Nu}}$	3.577	3.576	3.576	3.576	3.575	3.722	3.576
Case III	$\lvert\Psi_{max}\rvert$	2.499	2.499	2.499	2.499	2.499	2.499	2.499
	$\overline{\mathrm{Nu}}$	3.570	3.542	3.541	3.610	3.584	3.381	3.549
Case IV	$\lvert\Psi_{max}\rvert$	3.370	3.362	3.364	3.377	3.351	3.462	3.366
	$\overline{\mathrm{Nu}}$	4.613	4.610	4.611	4.616	4.590	4.914	4.611

Inspection of the numerical values of $|\Psi_{max}|$ in the conduction–dominated regime (i.e., Table 2 with Ra = 30) indicates that in Case I, increasing Nb leads to an insignificant growth in the flow strength (maximum 0.47%) but rising Nr or Nt causes a slight drop in it (maximum 1.15% and 1.46%, respectively). The results of Case II show that an increment in the thermophoresis number from 0.05 to 0.5 intensifies the flow strength to about 19.29%. Nb and Nr, however, contributes neutrally there. The results of Case III indicate that the value of $|\Psi_{max}|$ is not dependent in this case to Nb, Nr, and Nt. Meanwhile, notice that all current parameters are influential to the flow strength in Case IV. This is similar to Case I but the trends of the

Table 3. Numerical values of $|\Psi_{max}|$ and $\overline{\mathrm{Nu}}$ for the flow at Ra = 100

Ra = 100		Nb		Nr		Nt		$Nb = Nr = Nt$
		0.05	0.5	0.05	0.5	0.05	0.5	0.1
Case I	$\lvert\Psi_{max}\rvert$	4.707	4.725	4.722	4.676	4.722	4.668	4.717
	$\overline{\mathrm{Nu}}$	2.932	2.936	2.935	2.925	2.999	2.450	2.934
Case II	$\lvert\Psi_{max}\rvert$	2.618	2.622	2.622	2.608	2.579	2.942	2.621
	$\overline{\mathrm{Nu}}$	4.265	4.252	4.254	4.254	4.247	4.536	4.258
Case III	$\lvert\Psi_{max}\rvert$	3.264	3.240	3.245	3.288	3.237	3.342	3.251
	$\overline{\mathrm{Nu}}$	4.975	4.932	4.940	5.017	5.003	4.518	4.950
Case IV	$\lvert\Psi_{max}\rvert$	5.435	5.459	5.456	5.398	5.412	5.728	5.449
	$\overline{\mathrm{Nu}}$	5.512	5.500	5.503	5.530	5.468	5.987	5.506

Table 4. Numerical values of $|\Psi_{max}|$ and $\overline{\mathrm{Nu}}$ for the flow at Ra = 300

Ra = 300		Nb		Nr		Nt		$Nb = Nr = Nt$
		0.05	0.5	0.05	0.5	0.05	0.5	0.1
Case I	$\lvert\Psi_{max}\rvert$	9.813	9.847	9.841	9.749	9.843	9.709	9.831
	$\overline{\mathrm{Nu}}$	6.082	6.083	6.083	6.073	6.214	5.111	6.083
Case II	$\lvert\Psi_{max}\rvert$	6.270	6.286	6.284	6.181	6.222	6.756	6.282
	$\overline{\mathrm{Nu}}$	7.553	7.534	7.535	7.585	7.525	7.933	7.537
Case III	$\lvert\Psi_{max}\rvert$	8.02	7.952	7.958	8.094	7.953	8.094	7.981
	$\overline{\mathrm{Nu}}$	8.181	8.061	8.100	8.262	8.168	7.488	8.128
Case IV	$\lvert\Psi_{max}\rvert$	8.898	8.951	8.918	8.903	8.898	9.470	8.916
	$\overline{\mathrm{Nu}}$	8.800	8.904	8.831	8.981	8.799	9.721	8.830

variations are quite distinct. Evidently, with the increase in Nb, a slight drop in the flow strength appears (maximum 0.24%), but with an elevation in Nr or Nt, insignificant increases occur in it (maximum 0.39% and 3.31%, respectively).

Scrutiny of the $\overline{\mathrm{Nu}}$ values in Table 2 demonstrates that Nb and Nr possess a minor impact on the average Nusselt number in all current cases. Notice that maximum deviations of $\overline{\mathrm{Nu}}$, as a result of the tenfold increase in Nb and Nr, may not exceed 0.78% and 1.95%, respectively. The pattern is completely different when we go to Nt, since this parameter affects the heat transfer rate in all configurations. Specifically, a rise in Nt from 0.05 to 0.5 increases $\overline{\mathrm{Nu}}$ to 4.11% and 7.06% in Case II and Case IV with sinusoidal wall temperatures, but decreases it to 18.49% and 5.66% in Case I and Case III with constant wall temperatures, respectively. This controversy in the effect of the thermophoresis number on the heat transfer of cavities with uniform wall temperatures and those with non-uniform wall temperatures is in agreement with the previous findings in the natural convection environment, as pointed out previously.

The results presented in Table 3 belonging to Ra = 100 indicate that, in Case I, the variations of $|\Psi_{max}|$ with Nb, Nr and Nt are similar to those of Ra = 30. The corresponding deviations are +0.38%, −0.97%, and −1.14%, respectively. In Case II and III, the consequences of the pertinent parameters on the flow strength are no longer negligible at this Rayleigh number. In Case II, the tenfold increase in Nb, Nt, and Nr leads to 0.15% and 14.07% growths and a 0.53% drop in $|\Psi_{max}|$, respectively. The deviations are −0.74%, +3.24%, and +1.33% in Case III and +0.44%, +5.84%, and −1.06% in Case IV, respectively. Analysis of the average Nusselt number is also interesting. Similarly to what appeared at Ra = 30, it is evident that Nb and Nr are not so influential on $\overline{\mathrm{Nu}}$ prediction at Ra = 100. Maximum changes of $\overline{\mathrm{Nu}}$ by increasing Nb and Nr are +0.14% and −0.34% in Case I, −0.30% and 0% in Case II, −0.86% and +4.93% in Case III, and −0.22% and +0.49% in Case IV, respectively. The effect of the theromophoresis number on

the heat transfer rate is more remarkable. Specifically, a rise in Nt from 0.05 to 0.5 increases $\overline{\mathrm{Nu}}$ to 6.80% and 9.49% in Case II and IV but decreases it to 18.31% and 9.69% Case I and III, respectively.

Table 4 indicates that when Ra = 300, then Nb, Nr, and Nt affect the value $|\Psi_{max}|$ in all the problems. Notice that maximum variations of $|\Psi_{max}|$ as a result of the increase in Nb are +0.35%, +0.26%, −0.85% and +0.60% in Case I, II, III, and IV, respectively. The corresponding values due to a rise in Nr are −0.93%, −1.64%, +1.71%, and −0.17%. The results also demonstrates that a rise in Nt from 0.05 to 0.5 results in 8.58%, 1.77% and 6.43% increase in the flow strength in Case II, III, and IV, respectively, but decreases the value $|\Psi_{max}|$ to 1.36% in Case I.

Numerical values of the average Nusselt number in Table 4 indicate that an increase in Nb from 0.05 to 0.5 leads to +0.02%, +0.01%, −1.47%, and +1.18% deviations in heat transfer in Case I, II, III, and IV, respectively. The corresponding changes due to a rise in Nr are −0.16%, +0.66%, +2.0%, and +1.70%. The alternation of Nt also brings −17.75%, +5.42%, -8.33%, and +10.48% variations in the average Nusselt number.

The thermophoresis parameter is found to be the most effective coefficient in the current cases. In order to provide a better picture about the consequences of this parameter on distributions of isocontours of the stream function, temperature and nanoparticles fraction, the corresponding contours for the flow problems are provided in Figs. 2-5, which belong to Ra = 100 with both $Nt = 0.05$ and $Nt = 0.5$.

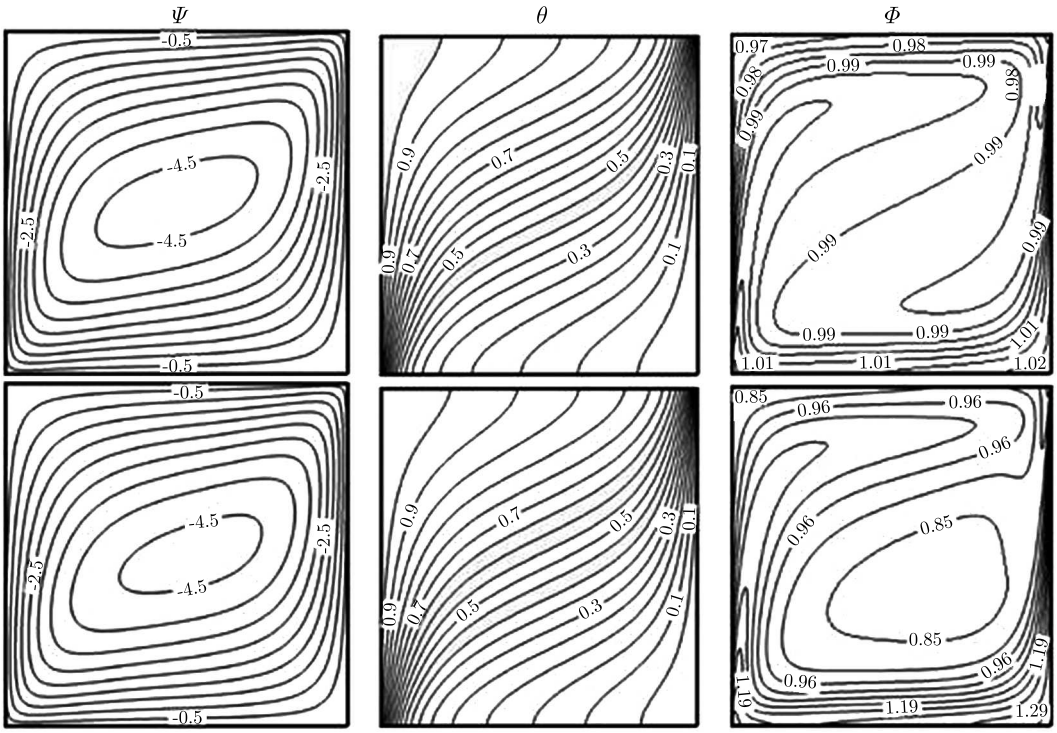

Fig. 2. Isocontours of the stream function, temperature and nanoparticles fraction for Case I at Ra = 100, Le = 25 with different values of Nt (up: $Nt = 0.05$; down: $Nt = 0.5$)

Figure 2 shows the isocontours of the stream function (left), temperature (middle) and nanoparticles fraction (right) for Case I. Regardless of the value of Nt, a single convective cell appears inside the cavity with an ascending flow near the left wall and a descending flow near the right wall. It is evident that a growth in Nt does not have a significant effect on the streamlines and isothermal lines but makes the nanoparticles distribution more non-homogeneous.

The streamlines, isotherms and isoconcentrations of Case II are provided in Fig. 3. Obviously, four convective cells appear here within the cavity. The convective cells located in the

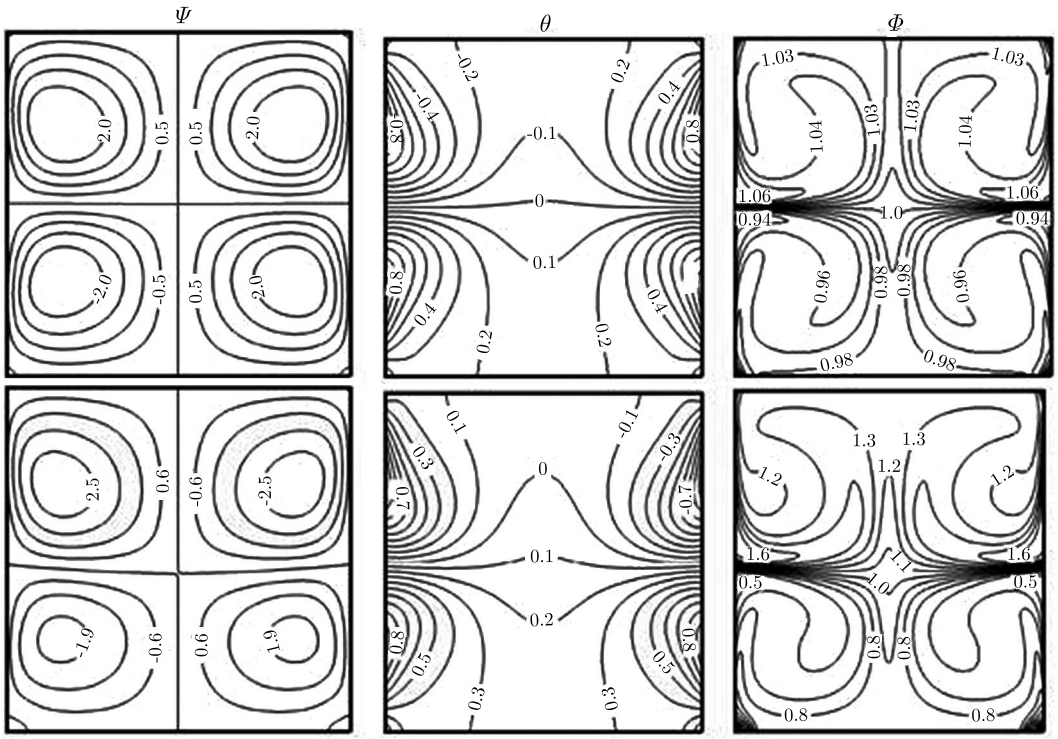

Fig. 3. Isocontours of the stream function, temperature and nanoparticles fraction for Case II at Ra = 100, Le = 25 with different values of Nt (up: $Nt = 0.05$; down: $Nt = 0.5$)

bottom-left/top-right parts of the cavity are rotating clockwise but those located in the bottom--right/top-left parts are counter-clockwise vortices. The appearance of these circulations is attributed to the imposition of the sinusoidal temperature distribution on the side walls in this case. Cores of the convective cells are located close to the side walls due to large temperature gradients there. The distributions of Ψ and θ are symmetric with respect to $X = 0.5$. It is evident that the Nt promotion leads to variations in all characteristics noticeably. Obviously, the streamlines pattern is changed in a way of growing the two top convective cells. Moreover, the bottom half of the cavity experiences more intensive heating while the opposite side transfers less heat. The main variations with Nt are related to the isoconcentrations. The Nt elevation causes a more non-homogeneous nanoparticles distribution. This is similar to Case I, but the effect is more remarkable here.

Figures 4 and 5 depict the isocontours of the stream function, temperature and nanoparticles fraction for Case III and IV, respectively. They correspond to the mixed convection environment. The effect of the Nt promotion on the distribution of the contour plots bears a strong resemblance to what is observed in the natural convection cases.

5. Concluding remarks

A critical analysis of natural and mixed convection of a nanofluid in square porous cavities has been presented here using Buongiorno's mathematical model. The findings of this study can be summarized as:

(1) Imposition of a sinusoidal temperature distribution on the sidewalls leads to heat transfer improvement both in the natural and mixed convection environments.

(2) The consequence of the thermophoresis number on the flow strength and the average Nusselt number is more prominent than the Brownian diffusion parameter and the thermophoresis number.

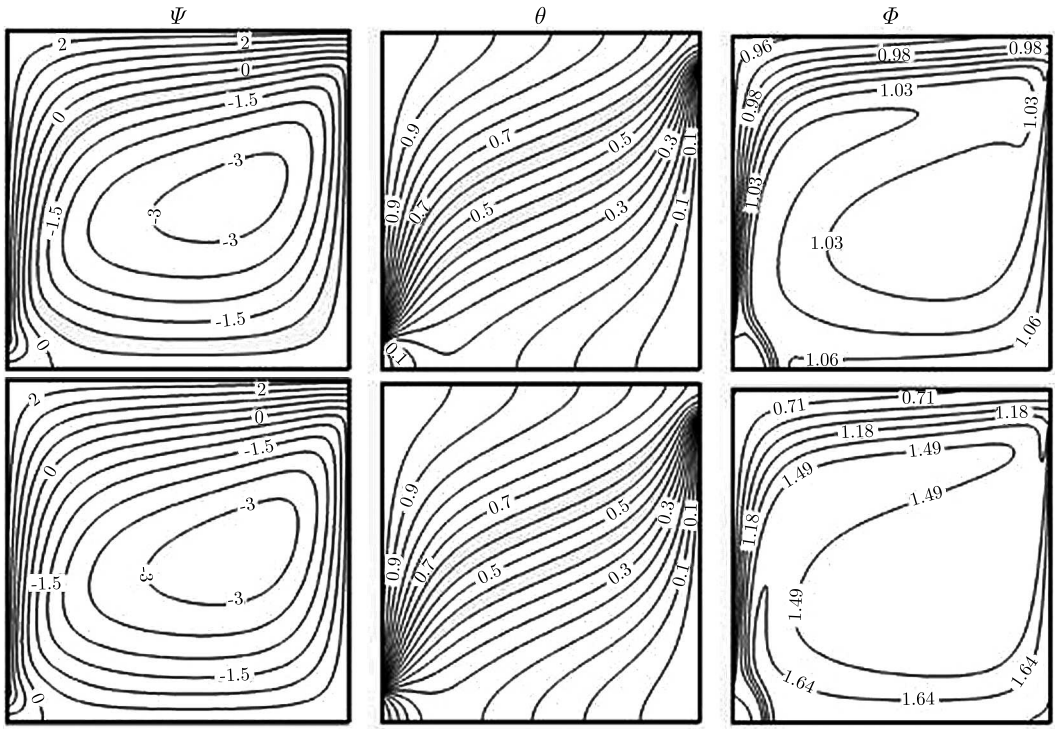

Fig. 4. Isocontours of stream the function, temperature and nanoparticles fraction for Case III at Ra = 100, Pe = 25, Le = 25 with different values of Nt (up: $Nt = 0.05$; down: $Nt = 0.5$)

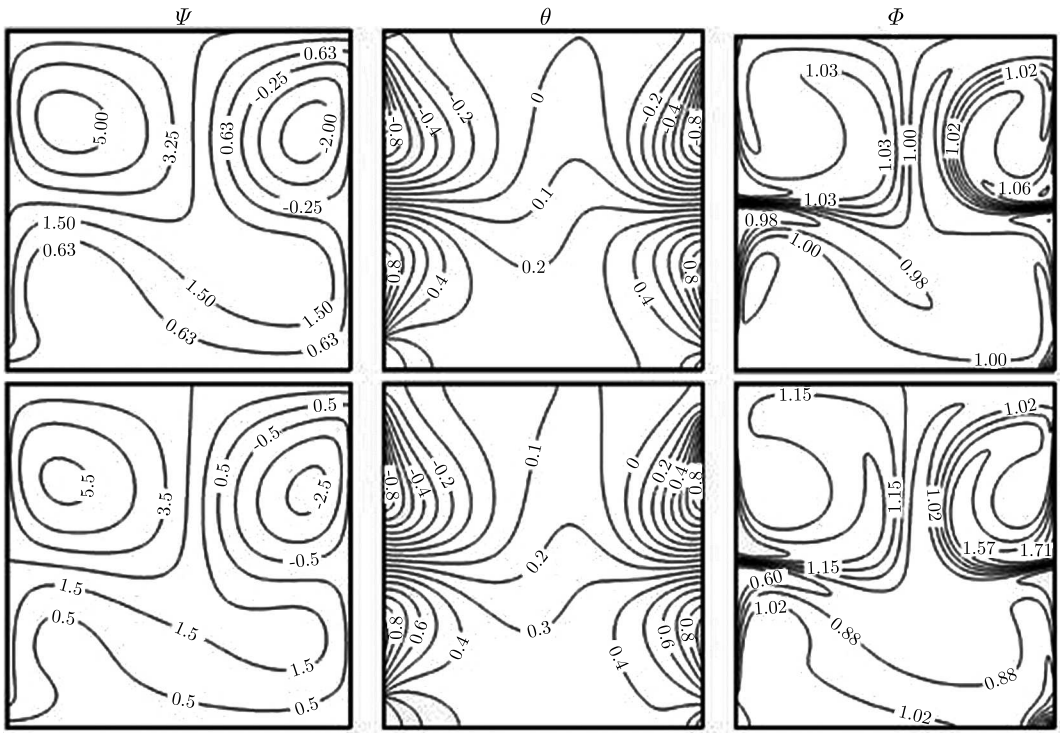

Fig. 5. Isocontours of the stream function, temperature and nanoparticles fraction for Case IV at Ra = 100, Pe = 25, Le = 25 with different values of Nt (up: $Nt = 0.05$; down: $Nt = 0.5$)

(3) With an increase in the thermophoresis number, progressive changes occur in the isocontours of the stream function, temperature and nanoparticles fraction, and the nanoparticles distribution becomes more non-homogeneous.
(4) With the sinusoidal wall temperatures, the heat transfer rate is an increasing function of the thermophoresis number, but in a cavity with uniform wall temperatures, depending on the value of the Rayleigh number, an increase in Nt may enhance or deteriorate the average Nusselt number.
(5) The Brownian diffusion parameter and the buoyancy ratio have almost no effect on $\overline{\mathrm{Nu}}$ in the natural convection but with an increase in Ra, they become gradually more influential in the mixed convection.

References

1. Ali K., Iqbai M.F., Akbar Z., Ashraf M., 2014, Numerical simulation of unsteady water--based nanofluid flow and heat transfer between two orthogonally moving porous coaxial disks, *Journal of Theoretical and Applied Mechanics*, **52**, 1033-1046
2. Behroyan I., Vanaki S.M., Ganesan P., Saidur R., 2016, A comprehensive comparison of various CFD models for convective heat transfer of Al2O3 nanofluid inside a heated tube, *International Communications in Heat and Mass Transfer*, **70**, 27-37
3. Buongiorno J., 2006, Convective transport in nanofluids, *Journal of Heat Transfer*, **128**, 240-250
4. Ghalambaz M., Sabour M., Pop I., 2016, Free convection in a square cavity filled by a porous medium saturated by a nanofluid: Viscous dissipation and radiation effects, *Engineering Science and Technology*, **19**, 1244-1253
5. Ghasemi S.E., Hatami M., Salarian A., Domairry G., 2016, Thermal and fluid analysis on effects of a nanofluid outside a stretching cylinder with magnetic field using the differential quadrature method, *Journal of Theoretical and Applied Mechanics*, **54**, 517-528
6. Kefayati G.H.R., 2017a, Mixed convection of non-Newtonian nanofluid in an enclosure using Buongiorno's mathematical model, *International Journal of Heat and Mass Transfer*, **108**, 1481-1500
7. Kefayati G.H.R., 2017b, Simulation of natural convection and entropy generation of non--Newtonian nanofluid in a porous cavity using Buongiorno's mathematical model, *International Journal of Heat and Mass Transfer*, **112**, 709-744
8. Mustafa M., 2017, MHD nanofluid flow over a rotating disk with partial slip effects: Buongiorno model, *International Journal of Heat and Mass Transfer*, **108**, 1910-1916
9. Nield D.A., Bejan A., 2013, *Convection in Porous Media*, Springer, New York
10. Nield D.A., Kuznetsov A.V., 2009, The Cheng-Minkowycz problem for natural convective boundary-layer flow in a porous medium saturated by a nanofluid, *International Journal of Heat and Mass Transfer*, **52**, 5792-5795
11. Rostamzadeh A., Jafarpur K., Goshtasbi Rad E., 2016, Numerical investigation of pool nucleate boiling in nanofluid with lattice Boltzmann method, *Journal of Theoretical and Applied Mechanics*, **54**, 3, 811-825
12. Sheikholeslami M., Ganji D.D., Rashidi M.M., 2016, Magnetic field effect on unsteady nanofluid flow and heat transfer using Buongiorno model, *Journal of Magnetism and Magnetic Materials*, **416**, 164-173
13. Sheremet M.A., Cimpean D.S., Pop I., 2017, Free convection in a partially heated wavy porous cavity filled with a nanofluid under the effects of Brownian diffusion and thermophoresis, *Applied Thermal Engineering*, **113**, 413-418

14. Sheremet M.A., Grosan T., Pop I., 2014, Free convection in shallow and slender porous cavities filled by a nanofluid using Buongiorno's model, *Journal of Heat Transfer*, **136**, 082501-1

15. Sheremet M.A., Pop I., 2014a, Conjugate natural convection in a square porous cavity filled by a nanofluid using Buongiorno's mathematical model, *International Journal of Heat and Mass Transfer*, **79**, 137-145

16. Sheremet M.A., Pop I., 2014b, Natural convection in a square porous cavity with sinusoidal temperature distributions on both side walls filled with a nanofluid: Buongiorno's mathematical model, *Transport in Porous Media*, **105**, 411-429

17. Sheremet M.A., Pop I., 2015a, Free convection in a triangular cavity filled with a porous medium saturated by a nanofluid Buongiorno's mathematical model, *International Journal of Numerical Methods for Heat and Fluid Flow*, **25**, 1138-1161

18. Sheremet M.A., Pop I., 2015b, Free convection in a porous horizontal cylindrical annulus with a nanofluid using Buongiorno's model, *Computers and Fluids*, **118**, 182-190

19. Sheremet M.A., Pop I., Rahman M.M., 2015, Three-dimensional natural convection in a porous enclosure filled with a nanofluid using Buongiorno's mathematical model, *International Journal of Heat and Mass Transfer*, **82**, 396-405

20. Torshizi E., Zahmatkesh I., 2016, Comparison between single-phase, two-phase mixture, and Eulerian-Eulerian models for the simulation of jet impingement of nanofluids, *Journal of Applied and Computational Sciences in Mechanics*, **27**, 55-70

21. Zahmatkesh I., 2008a, On the importance of thermal boundary conditions in heat transfer and entropy generation for natural convection inside a porous enclosure, *International Journal of Thermal Sciences*, **47**, 339-346

22. Zahmatkesh I., 2008b, On the importance of thermophoresis and Brownian diffusion for the deposition of micro- and nanoparticles, *International Communications in Heat and Mass Transfer*, **35**, 369-375

23. Zahmatkesh I., 2015, Heatline visualization for buoyancy-driven flow inside a nanofluid-saturated porous enclosure, *Jordan Journal of Mechanical and Industrial Engineering*, **9**, 149-157

24. Zahmatkesh I., Naghedifar S.A., 2017, Oscillatory mixed convection in jet impingement cooling of a horizontal surface immersed in a nanofluid-saturated porous medium, *Numerical Heat Transfer, Part A*, **72**, 401-416

Manuscript received August 19, 2017; accepted for print September 18, 2018